

Article

# Effect of Different Zigzag Channel Shapes of PCHEs on Heat Transfer Performance of Supercritical LNG

Zhongchao Zhao \*, Yimeng Zhou, Xiaolong Ma, Xudong Chen, Shilin Li and Shan Yang

School of Energy and Power, Jiangsu University of Science and Technology, Zhenjiang 212000, China; ymzhou@stu.just.edu.cn (Y.Z.); marlon@stu.just.edu.cn (X.M.); xudongchen@stu.just.edu.cn (X.C.); shilinli@stu.just.edu.cn (S.L.); shanyang33@stu.just.edu.cn (S.Y.)

\* Correspondence: zhongchaozhao@just.edu.cn; Tel.: +86-0511-84493050

Received: 10 May 2019; Accepted: 30 May 2019; Published: 31 May 2019



**Abstract:** The channels of a printed circuit heat exchanger (PCHE) can have different shapes, and the zigzag channel shape is one of the most widely used because of the relatively simple manufacturing process and low cost. However, the heat transfer enhancement of a zigzag channel is at the expense of increasing the pressure drop. In this paper, new channel shapes of a PCHE, i.e., a zigzag with an inserted straight channel and a zigzag channel with radian, were numerically investigated, with the aim of improving the heat transfer and reducing the pressure drop of supercritical LNG using the SST  $\kappa$ - $\omega$  model. The local and total pressure drop and heat transfer performance of supercritical LNG in a zigzag channel, zigzags with 1–5 mm inserted straight channels, and a zigzag channel with radian were analyzed by varying the mass flow rate from  $1.83 \times 10^{-4}$  to  $5.49 \times 10^{-4}$  kg/s. Performance evaluation criteria (PEC) were applied to compare the overall heat transfer performance of the zigzags with 1–5 mm inserted straight channels and a zigzag channel with radian to the zigzag channel of a PCHE. The maximum pressure drop for the zigzag channel was twice the minimum pressure drop for the zigzag channel with radian, while the convective heat transfer coefficient of the zigzag with a 4 mm inserted straight channel was higher, which was 1.2 times that of the zigzag channel with radian with the smallest convective heat transfer coefficient. The maximum value of the PEC with 1.099 occurred at a mass flow rate of  $1.83 \times 10^{-4}$  kg/s for the zigzag with a 4 mm inserted straight channel, while the minimum value of the PEC with 1.021 occurred at a mass flow rate of  $5.49 \times 10^{-4}$  kg/s for the zigzag with a 1 mm inserted straight channel. The zigzag with a 4 mm inserted straight channel had the best performance, as it had a higher PEC value at lower mass flow rates.

**Keywords:** printed circuit heat exchanger; supercritical LNG; zigzag channel; heat transfer performance

## 1. Introduction

Due to the technology of photochemical etching for the channel and the diffusion bonding for the stacking of plates, the channel size of the printed circuit heat exchanger (PCHE) is reduced to 1–3 mm resulting in PCHEs being very compact with a large heat transfer area and low temperature and high pressure bearing capacity [1–3]. Due to these advantages, PCHEs are suitable in volume-limited applications, such as a vaporizer [4].

PCHEs can have two types of channel—continuous and discontinuous structures. The continuous channel type includes the straight channel, zigzag channel, and wave channel, and the discontinuous channel consists of noncontinuous S-shaped and airfoil fins [5]. Chen et al. [6] numerically studied the steady-state and transient thermal performance using helium in a straight channel PCHE and experimentally verified the applicability of the dynamic model of the PCHE for simulating its performance. Mylavarapu et al. [7] investigated both numerically and experimentally the straight channel PCHE. The experimental heat transfer and pressure drop data were compared with the available

models and correlations. The pressure drop and Fanning friction factor were obtained at laminar and laminar-to-turbulent transition flow regimes numerically. Chen et al. [8] studied numerically and experimentally a zigzag PCHE using helium as the working fluid. The dynamic response of the PCHE was analyzed, and transient tests were experimentally carried out. The comparison between the simulation and experimental data proved the reliability of the dynamic model. Zheng et al. [9] studied transient heat transfer in a semicircular zigzag channel at laminar flow with Reynolds numbers (Re) of 400–800 and Prandtl numbers of 0.7–20. They found that both the heat transfer enhancement and the pressure drop rise as the Re increases, and the enhancement of the heat transfer is inversely proportional to  $Pr^{1/3}$ . Lee et al. [10] used three-dimensional RANS analysis and a hybrid multiobjective evolutionary algorithm coupled with the RSA model to optimize the zigzag channel of a PCHE to enhance the heat exchange effectiveness and reduce frictional loss. Kim et al. [11] developed the Fanning factor and Nusselt number correlations by considering the parameters that significantly affect the thermal hydraulic performance of a PCHE, such as angle, pitch, and hydraulic diameter. Yang et al. [12] numerically investigated a wavy channel PCHE, studied the effect of narrowing channel cross-sections on the thermal hydraulic performance, and proposed new heat transfer and frictional factor empirical correlations. Tsuzuki et al. [13] numerically investigated the effect of the fin angle, overlapping length, fin width, fin length, and edge roundness of S-shaped fins on the thermal hydraulic characteristics of a microchannel heat exchanger. Chu et al. [14] ran a numerical simulation of the airfoil fins' geometrical structure. They analyzed the dynamic performance and heat transfer characteristics with different pitches and fitted the correlations of  $j$  and  $f$  factors.

Based on previous research, considering the manufacturing process and the cost, the zigzag channel has been widely used in PCHEs [3,5,11]. However, the heat transfer of zigzag channels is 1.2 times and the pressure drop is 1.5 times that of straight channels [15]. The increase in heat transfer capacity is accompanied by a larger increase in pressure drop. Therefore, it is necessary to decrease the zigzag channel's pressure drop performance and improve its heat transfer performance.

At present, there are two ways to increase the heat transfer performance and decrease the pressure drop. One way is to optimize the structure; the other is to replace the traditional fluid with a supercritical fluid [16,17]. Several studies have used carbon dioxide and helium on PCHEs as the working fluid [18–20]. However, supercritical CO<sub>2</sub> is considered as the working fluid in the Brayton cycle for high temperature gas-cooled reactors (HTGRs) because of its high density, low viscosity, and high thermal conductivity [5,21,22], while only a few studies using supercritical LNG on a PCHE vaporizer exist [16].

In our previous work [23], the influence of a zigzag channel's bending angles in a PCHE on the heat transfer performance of supercritical LNG was numerically investigated, and the study found that the heat transfer and the pressure drop of supercritical LNG were highest at a bending angle of 45°. The present paper, based on the zigzag channel with a bending angle of 45°, proposes new types of channels in a PCHE, i.e., a zigzag with an inserted straight channel and a zigzag channel with radian, to improve the heat transfer and reduce the pressure drop. Numerical analysis on the local and overall heat transfer performance and pressure drop for the zigzag, zigzags with 1–5 mm inserted straight channels, and the zigzag channel with radian was carried out within the range of  $1.83 \times 10^{-4}$  to  $5.49 \times 10^{-4}$  kg/s mass flow rate. To find the channel structure with the best heat transfer performance, comprehensive consideration of the heat transfer performance and pressure drop was made, and performance evaluation criteria (PEC) were proposed to compare the heat transfer performance of zigzags with different lengths of inserted straight channels and the zigzag channel with radian to the zigzag channel.

## 2. Numerical Methodology

### 2.1. Physical Description

This study numerically investigated the thermal hydraulic performance of LNG in three different geometries of the cold channel in a cross flow PCHE. Figure 1a shows the straight hot channel with R22

as a working fluid to eliminate the risk of freezing [24] and the cold channel with the supercritical LNG single banked in the cross-flow arrangement. The investigated structures of the cold channel were zigzag, zigzag with an inserted straight channel, and zigzag channel with radian. Since it is impossible to simulate the fluid flow in the whole PCHE, and with the supercritical LNG in the cold channel being investigated, the model needed to be simplified. The mass flow rate of each cold channel was assumed to be the same and that it was adiabatic between two adjacent cold channels. Therefore, the model was reduced to a cold channel (Figure 1b). The solid part was made of steel, with a  $2 \times 1.75$  mm section, and the diameter of the semicircular cold channel was 1.5 mm. A channel of 400 mm was divided into 20 pitches along the flow direction with 20 mm as the unit, and each pitch was expressed by  $N_p$ . Figure 2 shows the geometric size of the three channel shapes; the bending angles of all the channels were designed to be  $45^\circ$ .

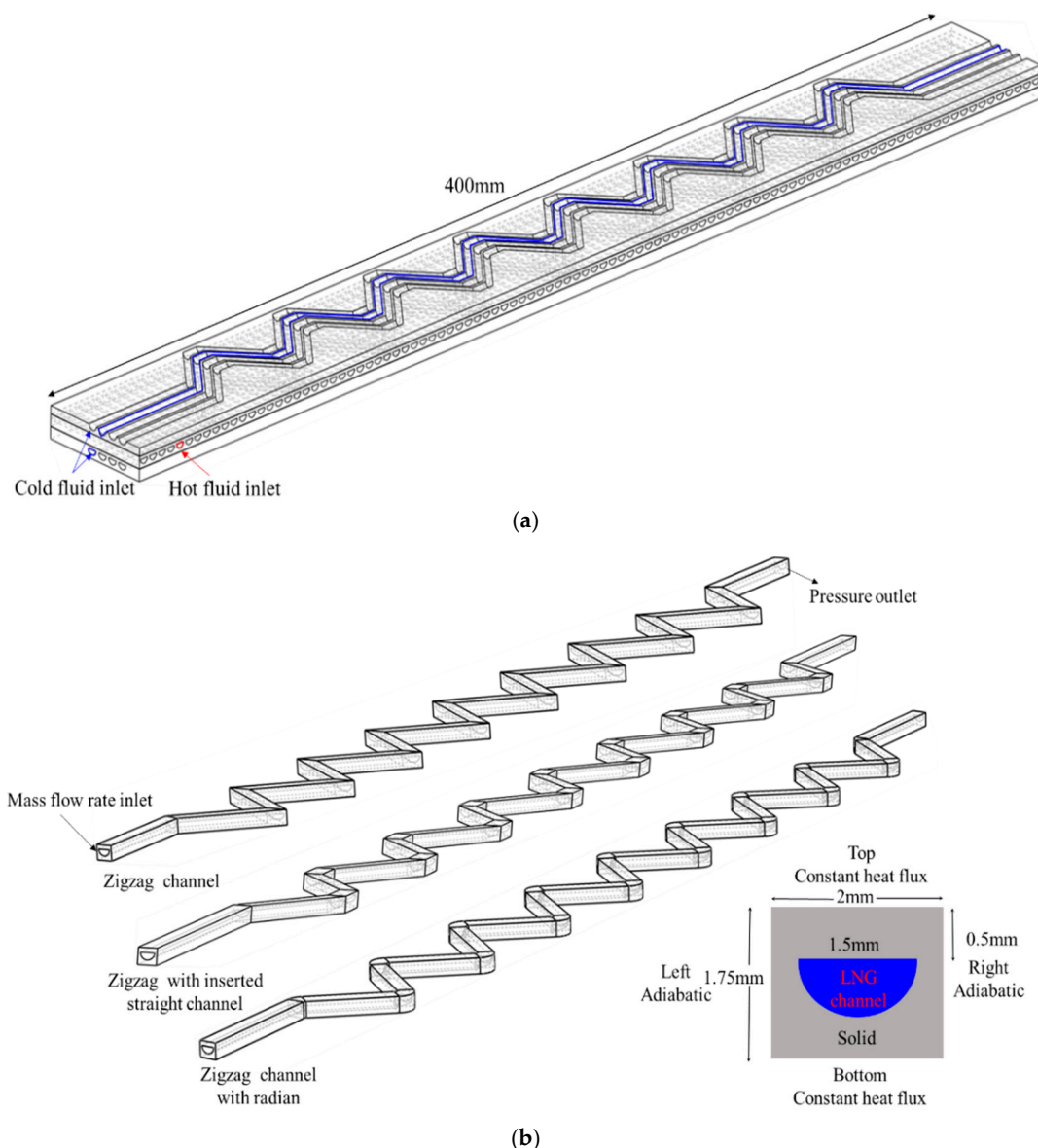


**Figure 1.** The simplified numerical model: (a) the core of PCHE; (b) the shape of a single channel and boundary conditions.

Figure 1b shows the model's boundary conditions. The mass flow rate was set to be the inlet boundary condition, and the outlet boundary condition was set by the pressure outlet. A constant heat

flux boundary condition was applied to the top and bottom walls, while the left and right walls were the adiabatic boundary condition. Table 1 summarizes the information for the boundary conditions.

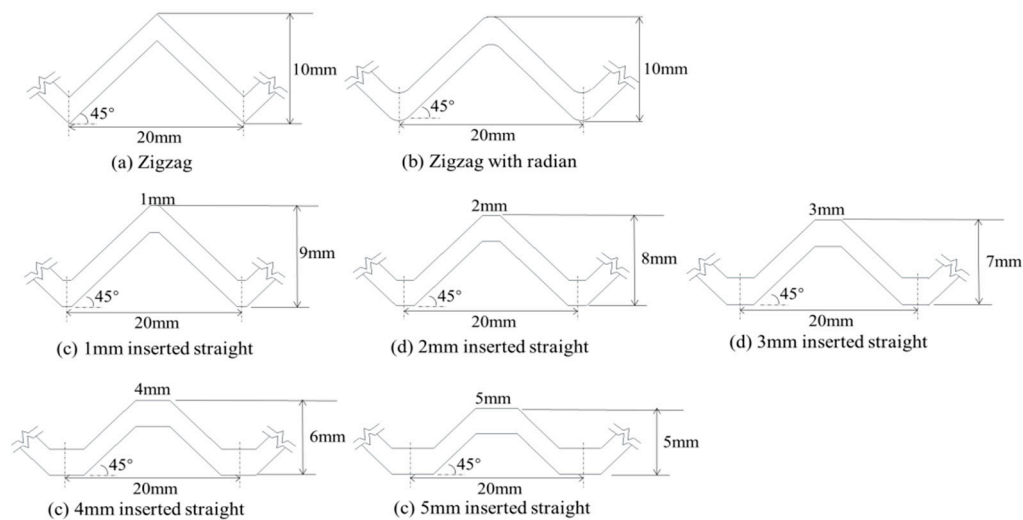


**Figure 2.** Geometric sizes of the zigzag channel, the zigzags with the inserted straight channels, and the zigzag channel with radian.

**Table 1.** Details of boundary conditions.

Inlet		Outlet		Top/Bottom Walls
Pressure (MPa)	Temperature (K)	Mass flow rate (kg/s)	Pressure outlet	Constant heat flux ( $W/m^2$ )
10	121	$1.83 \times 10^{-4}$		$7.5 \times 10^4$

## 2.2. Thermo-Physical Properties of Supercritical LNG

Compared with conventional fluids, the temperature affects the thermal physical properties of supercritical LNG significantly, and some special changes occur. Figure 3 shows the changes in density, specific heat, thermal conductivity, and dynamic viscosity with temperature from 121 K to 385 K at 10 MPa. Near the pseudo-critical temperature, the thermal physical properties vary severely. The thermal physical properties of supercritical LNG are referenced from the NIST Standard Reference Database (REFPROP) [25]. Since the properties vary dramatically as the temperature changes, the values were fitted as a piecewise-polynomial function of temperature, and the function was then associated with the ANSYS Fluent.

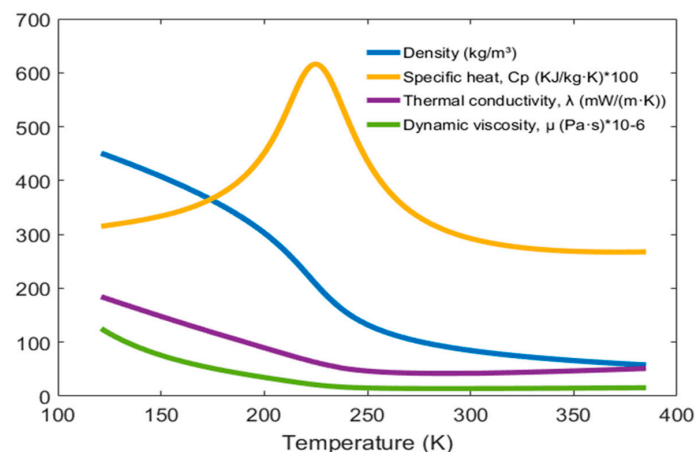


**Figure 3.** Thermo-physical properties of supercritical LNG at 10 MPa.

### 2.3. Numerical Method and Grid Independence

Commercial software ANSYS Fluent 14.5 was used for establishing the numerical model and run the simulation. The range of the average Re number was 7600–10,133, which was the turbulent flow condition. According to our previous work [23], the SST  $\kappa$ - $\omega$  model was chosen to calculate the supercritical fluids. The details of the SST  $\kappa$ - $\omega$  model are shown in the literature [26]. The coupling of velocity and pressure was set up by using the SIMPLE algorithm, because the error between the simulation results calculated by the SIMPLE algorithm and the experimental results was smaller than in other algorithms, and the second-order upwind scheme was applied to discretize the momentum, energy, turbulent kinetic energy, and turbulent dissipation rate equations. In addition, the calculations were considered to be convergent when the residual values were of  $10^{-6}$ .

The following governing equations of continuity, momentum, and energy were used in the calculation:

Continuity equation:

$$\frac{\partial}{\partial x_i}(\rho u_i) = 0, \quad (1)$$

Momentum equation:

$$\frac{\partial}{\partial x_i}(\rho u_i u_j) = -\frac{\partial p}{\partial x_i} + \rho g_i + \frac{\partial}{\partial x_j}[(\mu + \mu_t) \frac{\partial u_i}{\partial x_j}], \quad (2)$$

Energy equation:

$$\frac{\partial}{\partial x_i}(u_i(\rho E + p)) = \frac{\partial}{\partial x_i}\left(k_{eff} \frac{\partial T}{\partial x_i} + u_i \tau_{ij}\right), \quad (3)$$

$$k_{eff} = k + k_t$$

where  $\rho$  is density,  $u_i$  is the velocity vector,  $p$  is pressure,  $\mu$  and  $\mu_t$  are the molecular and turbulent viscosities, respectively,  $k_{eff}$  is effective conductivity, and  $k_t$  is turbulent thermal conductivity.

The local performance of heat transfer and the pressure drop are listed as follows:

$$\Delta P = P_{out} - P_{in}, \quad (4)$$

$$h = \frac{q}{T_w - T_b} = \frac{q}{T_w - (T_{out} + T_{in})/2}, \quad (5)$$

where  $P_{out}$  and  $P_{in}$  are the average pressure of the inlet and outlet, respectively,  $q$  is the constant heat flux,  $T_w$  and  $T_b$  are the wall temperature and average temperature, respectively, of the LNG at the inlet and the outlet.

$$Nu = \text{Nusselt number} = \frac{h D_h}{\lambda}, \quad (6)$$

$$D_h = \text{Hydraulic diameter} = 4A/l, \quad (7)$$

$$f = \text{Fanning friction coefficient} = \frac{\Delta P_f D_h}{2L \rho_b v_b^2}, \quad (8)$$

$$\Delta P_f = \Delta P - \Delta P_a = \Delta P - (\rho_{out} v_{out}^2 - \rho_{in} v_{in}^2) \quad (9)$$

where  $\lambda$  is thermal conductivity,  $A$  and  $l$  are the cross-sectional area and circumference of the semicircular fluid area, respectively,  $\Delta P_f$  and  $\Delta P_a$  are the frictional and accelerated pressure drops,  $L$  is the channel length, and  $\rho_b$  and  $v_b$  are the bulk density and velocity of the LNG, respectively.

The total Nusselt number ( $Nu$ ) and Fanning friction coefficient are calculated as follows:

$$Nu_t = \frac{1}{n} \sum_i^n Nu_i, \quad (10)$$

$$f_t = \frac{1}{n} \sum_i^n f_i, \quad (11)$$

where  $Nu_i$  and  $f_i$  are the average Nusselt number and Fanning friction coefficient of each channel pitch, respectively, and  $n$  is the number of the channel pitch.

The performance evaluation criteria (PEC) are defined as in Equation (12):

$$PEC = \frac{Nu_{t,i}}{Nu_{t,zigzag}} \left( \frac{f_{t,i}}{f_{t,zigzag}} \right)^{\frac{1}{3}}, \quad (12)$$

where the subscript  $t,zigzag$  is the total performance of the zigzag channel and  $t,i$  is the total performance of the other channel shapes.

The structured meshes for the model were generated by GAMBIT. For the semicircular fluid domain, the distance between the first layer and the interface was 0.01 mm, and the growth factor was set to 1.1 mm for the remaining rows. A grid independence study was performed for the zigzag channel. Figure 4 compares the influence of the size of the grid (i.e., 1.9, 2.6, 3.3, 3.7, 4.2, and 4.9 million nodes) on the temperature difference and pressure drop between the inlet and the outlet. When the number of nodes was greater than 3.9 million, the temperature difference and pressure drop barely changed. Hence, the mesh with 3.9 million nodes was selected.

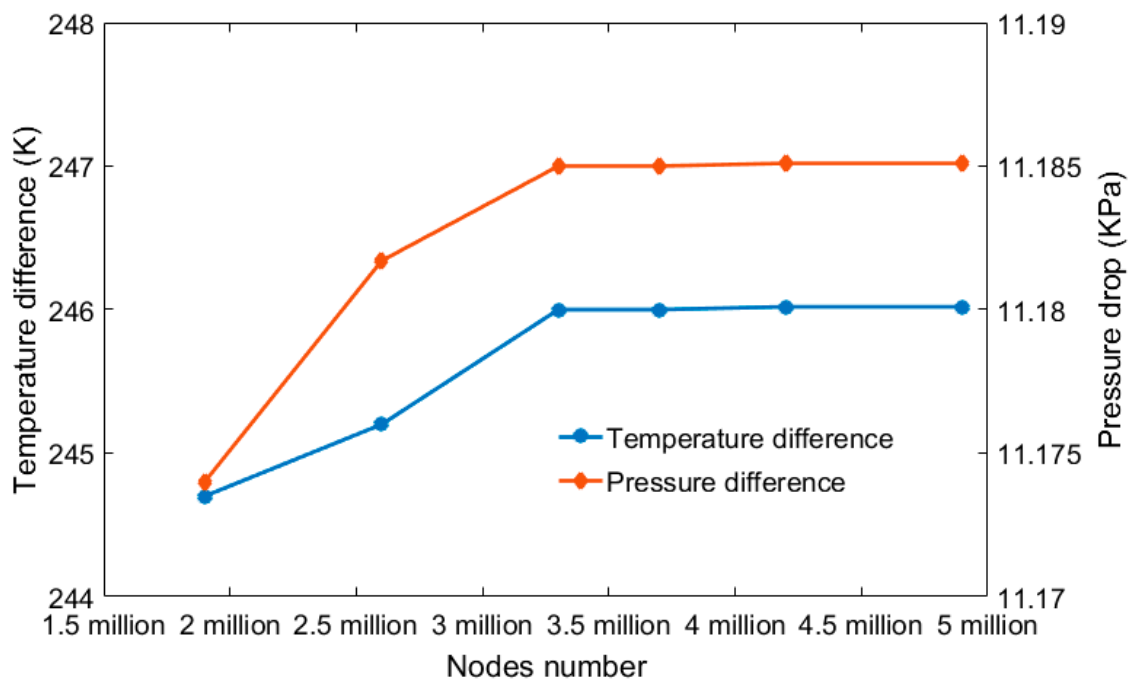


Figure 4. Grid independence test.

#### 2.4. Model Validation

In order to ensure the correctness of the simulation models and methods, the numerical results were compared to Zhao et al.'s experimental results [4]. A 520 mm long straight channel model with supercritical nitrogen as the working fluid was established, which was consistent with the experiment. In the simulation, the operating conditions, such as inlet temperature, inlet pressure, and mass flow rate of 102 K, 10 MPa, and  $1.83 \times 10^{-4}$  kg/s, respectively, were the same as the experimental conditions. Table 2 compares the experimental results with the simulation results and highlights that the relative error in temperature difference was 0.11% while the pressure drop was 3.82%, indicating that the numerical model and methods are applicable.

**Table 2.** Comparison between simulation and experimental results at 10 MPa: relative error.

Title	Simulation Results	Experiment Data	Relative Error (%)
Temperature difference $\Delta T$ (K)	186.4	186.6	0.11
Pressure difference $\Delta P$ (Pa)	10,189.45	10,578.6	3.82

### 3. Results and Discussion

Figure 5 shows the local pressure drop performance of different channel shapes; the pressure drop was highest for the zigzag channel (11.85 kPa). The pressure drops for the zigzag channels with inserted straight channels from 1 to 5 mm were 7.9, 7.1, 6.9, 6.7, and 6.5 kPa, respectively, while that for the zigzag channel with radian was the lowest (5.9 kPa). The pressure drop of the zigzag channel was 33–60% larger than the other channel shapes. For the zigzag with the inserted straight channel, the pressure drop decreased as the length of the inserted straight channel rose. This phenomenon can be explained as follows: (1) The velocity of LNG in the zigzag channel was significantly higher than that of the other channel shapes (Figure 6), which increased the pressure drop of the zigzag channel. (2) The flow separation and dead zones occurring in the channel led to an increase in the pressure drop. The dead zones of the zigzag channel were larger than the other channels. (3) The longer the path of the LNG flow through the channel, the greater the pressure drop. Compared to the other shapes, the LNG had the longest flow path and the greater pressure drop in the zigzag channel. For the zigzags with the inserted straight channels, although Figure 6 shows that the area of the dead zone increased as the inserted straight channel length increased, the LNG flowing path decreased as the inserted straight channel length increased. (4) The pressure drop was the minimum in the zigzag channel with radian. Due to the small dead zone in the channel, the velocity gradient and the disturbance of LNG were small, resulting in a small pressure drop.

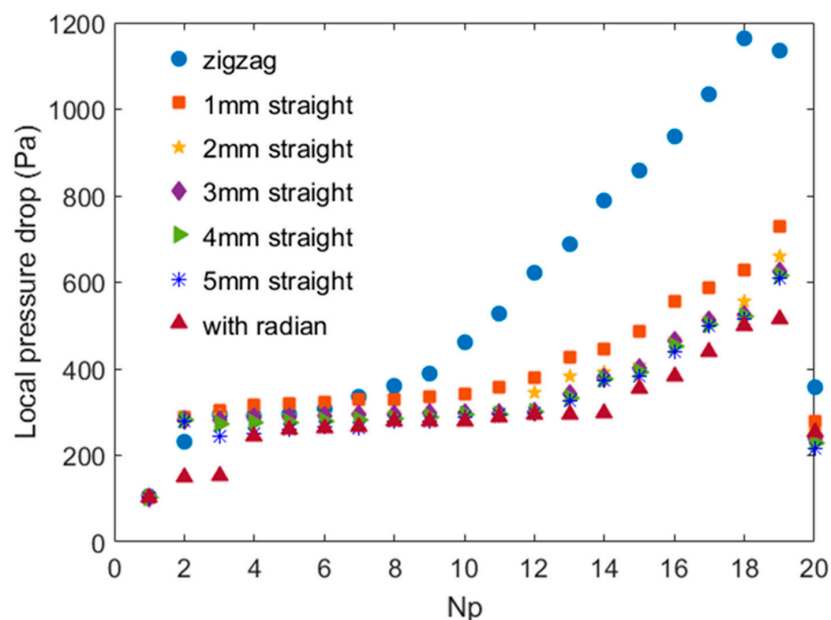
**Figure 5.** Local pressure drop along the flow direction for different channel shapes.

Figure 7 shows the local convection heat transfer coefficient along the flow direction for different channel shapes. The convection heat transfer coefficient was the highest for the zigzag with the inserted straight channel, especially after  $Np = 8$ . Moreover, the zigzag with the 1 mm inserted straight channel had the highest convection heat transfer coefficient. The channel with radian had a relative low convection heat transfer coefficient compared to the other channel shapes, maybe because the flow separation and the dead zone in the channel led to a reduction in the effective heat transfer area,

resulting in a reduced heat transfer capacity. In Figure 6, the flow separation and the dead zone of the zigzag with a 1 mm inserted straight channel is not obvious, on the contrary, the dead zone in the zigzag channel appears before and after the bending point. The dead area in the zigzag channel is the largest, and it is the smallest in the zigzag with the 1 mm inserted straight channel. With the increasing length of the straight channel, the dead area increases. The dead zone is similar in the zigzags with the 3, 4, and 5 mm inserted straight channels. The zigzag channel with radian had a lower convection heat transfer coefficient than the other channel shapes. Although the dead zone was not obvious in the zigzag channel with radian, the velocity gradient was also small, proving that the geometry influenced the fluid a little, leading to the reduction of the convection heat transfer coefficient in the zigzag channel with radian.

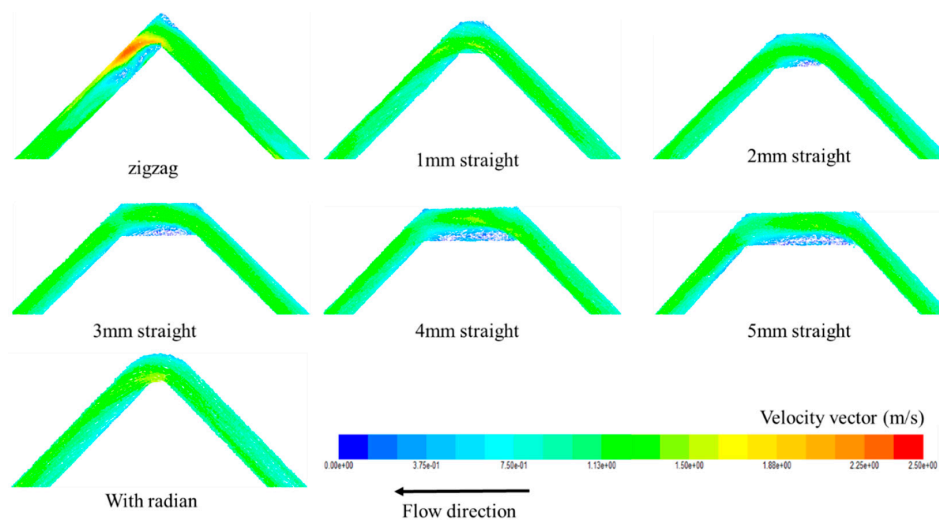


Figure 6. Velocity vectors for different channel shapes.

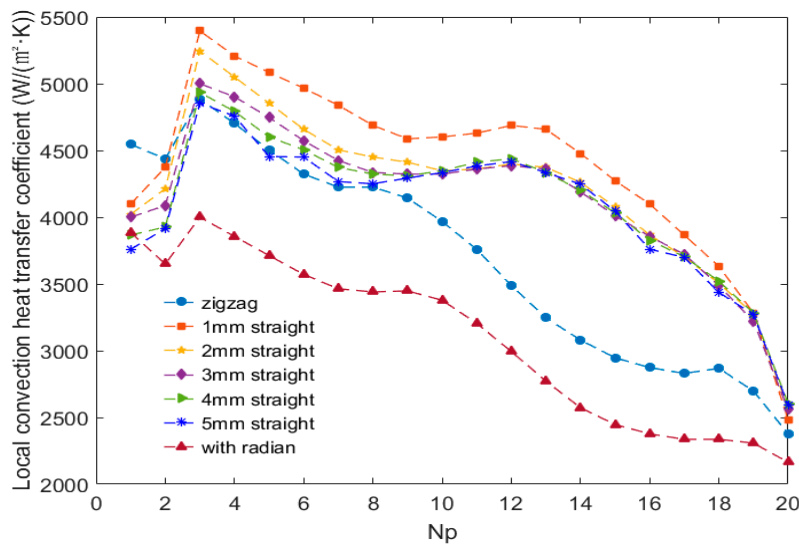
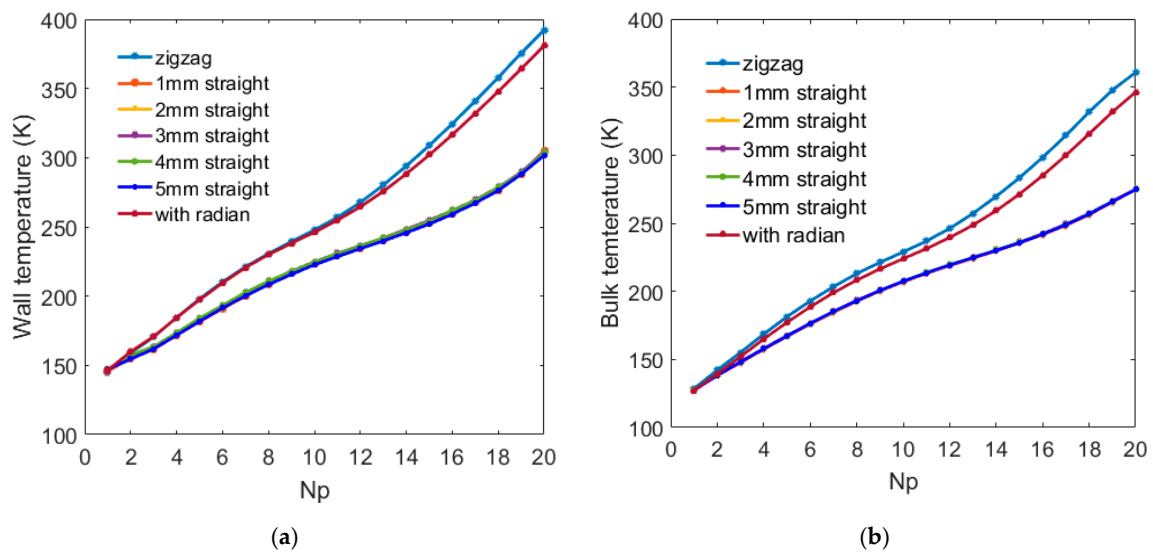


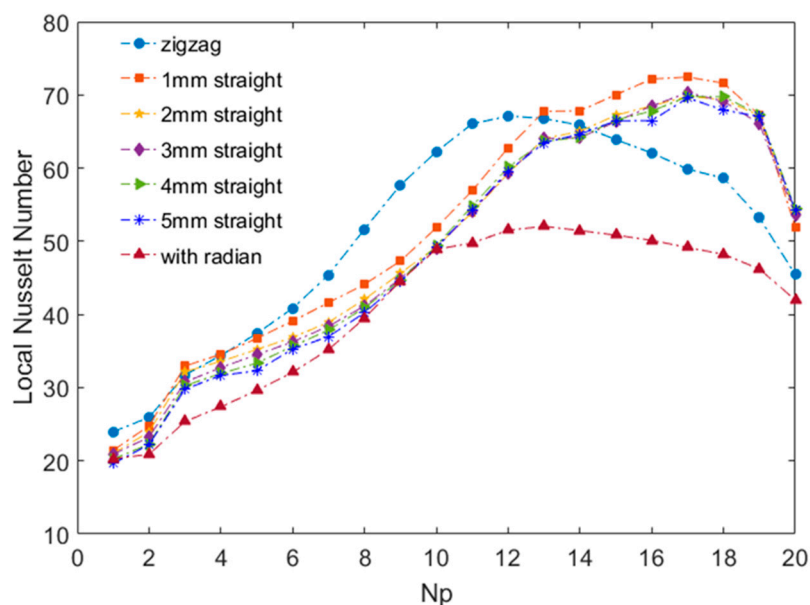
Figure 7. Local convection heat transfer coefficient along the flow direction for different channel shapes.

According to Equation (5), the convection heat transfer coefficient is inversely proportional to the difference between the wall temperature and the fluid bulk temperature. Figure 8 shows the wall temperature and the LNG bulk temperature for the different channel shapes. After  $Np = 8$ , the growth rate of the wall temperature is greater than the LNG bulk temperature for the zigzag channel and zigzag channel with radian; therefore, they both have a much smaller convection heat transfer coefficient.



**Figure 8.** (a) Wall temperature and (b) LNG bulk temperature for different channel shapes.

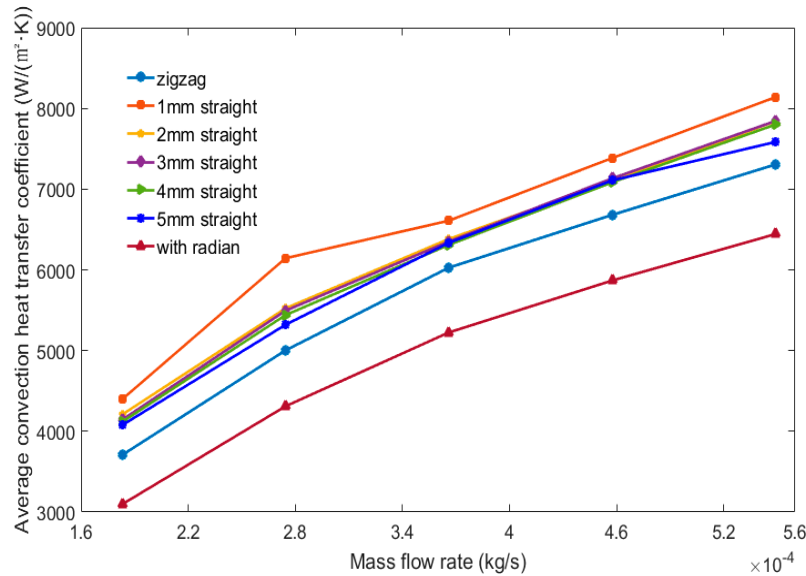
Figure 9 shows the Nusselt number ( $Nu$ ) along the flow direction for the different channel shapes. The  $Nu$  increases and then reduces along the flow direction, because it is inversely proportional to the thermal conductivity. With the rising temperature of the LNG along the flow direction, the thermal conductivity declines sharply and reaches the minimum near the pseudo-critical temperature, then rises slightly (see the purple line in Figure 3). In addition, the  $Nu$  of the zigzag channel and zigzag channel with radian reaches the maximum value near  $Np = 12$ , while that of the zigzags with inserted straight channels peaks at  $Np = 16$ . This difference is due to the LNG temperature of the zigzag channel and zigzag channel with radian rising faster and reaching the pseudo-critical temperature at  $Np = 12$ , while the LNG temperature of the zigzags with inserted straight channels rises slowly and reaches the pseudo-critical temperature at  $Np = 16$  (Figure 8b).



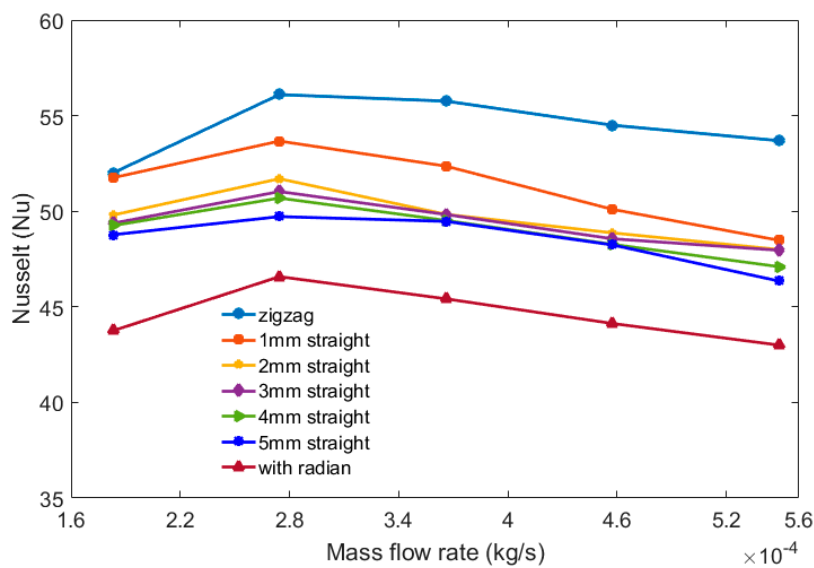
**Figure 9.** Nusselt number ( $Nu$ ) along the flow direction for different channel shapes.

Figure 10 shows the average convection heat transfer coefficient of different channel shapes at different mass flow rates. The average convection heat transfer coefficient was the highest in the zigzags with the inserted straight channels, while it was the lowest in the zigzag channel with radian.

As the mass flow rate rose from  $1.83 \times 10^{-4}$  to  $5.49 \times 10^{-4}$  kg/s, the average convection heat transfer coefficient of the different channel shapes increased due to the increase in turbulence. Figure 11 shows the trend of the Nusselt number of the different channel shapes when varying the mass flow rate:  $Nu$  increases and then decreases with the increase of the mass flow rate.



**Figure 10.** Average convection heat transfer coefficient of different channel shapes at different mass flow rates.



**Figure 11.**  $Nu$  of different channel shapes at different mass flow rates.

The Nusselt number at  $2.745 \times 10^{-4}$  kg/s was the maximum in all channel shapes, because as the mass flow rate increased, the heat absorbed by the fluid per unit volume from the solid decreased, resulting in a decrease of temperature, an increase of thermal conductivity, and a decrease of the  $Nu$ . The zigzags with the inserted straight channels had the largest average convection heat transfer coefficient, but the zigzag channel had a larger Nusselt number than the zigzags with the inserted straight channels. The temperature of the LNG was higher in the zigzag channel than that of the zigzags with the inserted straight channels, so the thermal conductivity was small, causing the  $Nu$  to become larger.

Figure 12 shows the total pressure drop, which was largest in the zigzag channel, whereas it was smallest in the zigzag channel with radian. The total pressure drop decreased as the inserted straight channel length increased. The pressure drop of the different channel shapes increased with the increase of the mass flow rate because of the rising velocity, as in Figure 13. Figure 14 shows the Fanning friction factor of the different channel shapes when varying the mass flow rate. The zigzag channel and the zigzag channel with radian had the largest and smallest Fanning friction coefficient, respectively. With the increasing length of the inserted straight channel, the Fanning friction coefficient decreased; also, the 3, 4, and 5 mm inserted straight channels had a similar Fanning friction coefficient. The Fanning friction coefficient reduced slightly as the mass flow rate increased. From Equation (8), the Fanning friction coefficient is inversely proportional to  $\rho_b v_b^2$ . According to Figure 3, as the mass flow rate increases, the LNG temperature decreases, and the density and viscosity increase. The increased velocity and density lead to the increase in  $\rho_b v_b^2$ , resulting in a reduction in the Fanning friction coefficient.

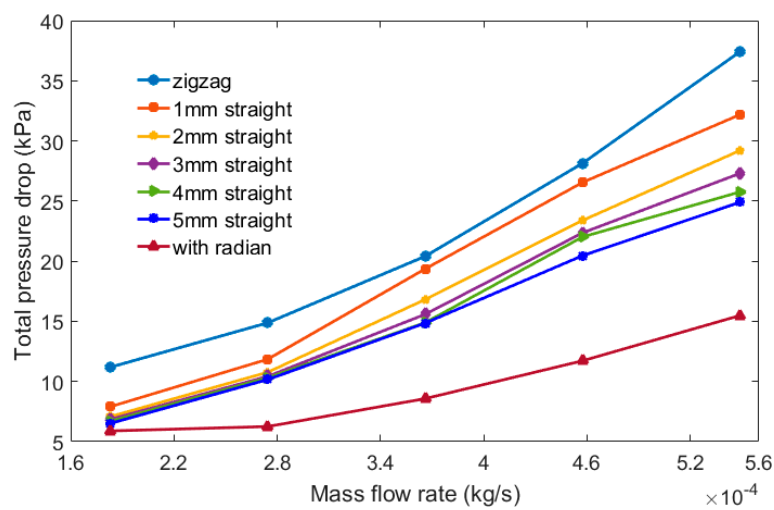


Figure 12. Total pressure drops for different channel shapes at different mass flow rates.

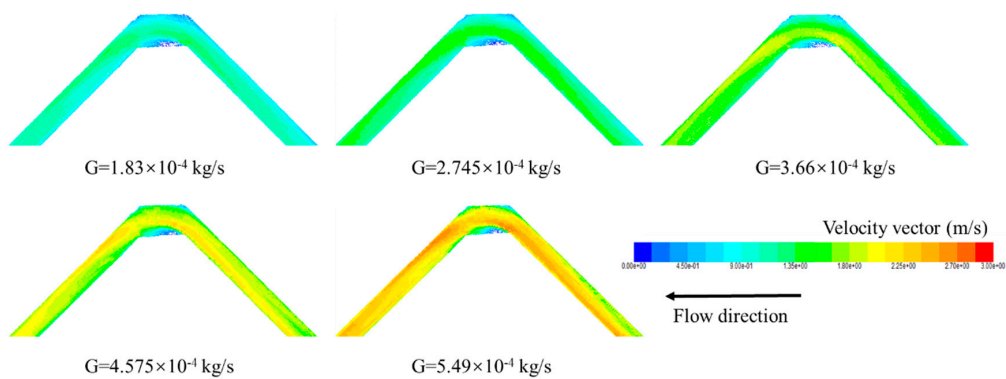


Figure 13. Velocity vectors of  $Np = 10$  at different mass flow rates.

In order to compare the comprehensive heat transfer performance of the different channel shapes, performance evaluation criteria (PEC) were proposed to evaluate the heat transfer performance and pressure drop performance of the different channel shapes. Figure 15 shows the PEC for the zigzags with the inserted straight channels and the zigzag channel with radian. The PEC were all greater than 1, indicating that the comprehensive heat transfer performance of the LNG in these channels was better than the traditional zigzag channel. The PEC were higher at a lower mass flow rate. The maximum value of the PEC corresponds to a mass flow rate of  $1.83 \times 10^{-4}$  kg/s for the zigzags with the 4 and 5 mm inserted straight channels, while the minimum corresponds to the mass flow rate of  $5.49 \times 10^{-4}$  kg/s

for the zigzag with the 1 mm inserted straight channel. The maximum and minimum values were 1.099 and 1.021, respectively. In summary, the results show that the zigzags with the inserted straight channels and the zigzag channel with radian had the best performance, which had higher PEC at lower mass flow rates. The zigzag with the 4 mm inserted straight channel had the greatest heat transfer performance.

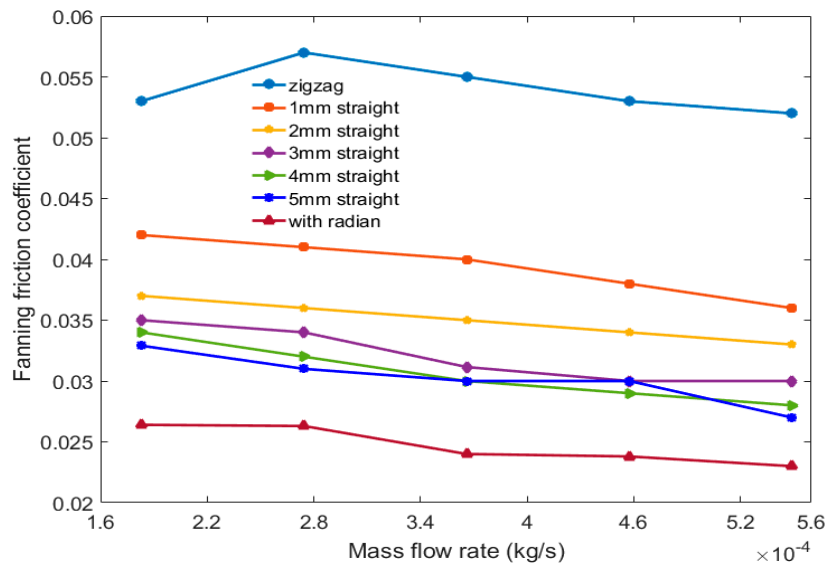


Figure 14. Fanning friction factor for different channel shapes at different mass flow rates.

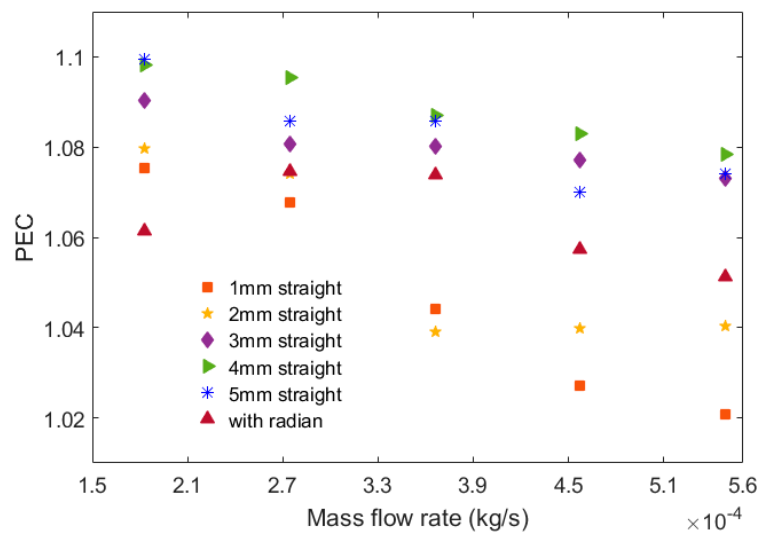


Figure 15. Performance comparison for different channels at different mass flow rates.

#### 4. Conclusions

In this study, the heat transfer and pressure drop performance of supercritical LNG in the zigzag channel, zigzags with inserted straight channels, and the zigzag channel with radian were discussed. Performance evaluation criteria were introduced to combine the heat transfer and pressure drop performance in order to compare the heat transfer performance of three different types of channel shape. Based on the results above, the following conclusions can be drawn:

- (1) The following factors affecting the pressure drop can be summarized: (a) increasing velocity leads to an increase in pressure drop, (b) the flow separation and dead zones occurring in the channel increase the pressure drop, (c) the longer the path of the LNG flowing through the

- channel, the greater the pressure drop, and (d) the stronger the channel disturbance on the fluid, the greater the pressure drop;
- (2) The pressure drop is largest in the zigzag channel, while it is smallest in the zigzag channel with radian. For the zigzags with the inserted straight channels, as the inserted straight channel length increases, the pressure drop decreases;
  - (3) The convection heat transfer coefficient is largest in the zigzag with the inserted straight channel, and it is higher in the zigzag with 1 mm inserted straight channel. The zigzag channel with radian has a relative low convection heat transfer coefficient;
  - (4) With the mass flow rate within the range  $1.83 \times 10^{-4}$ – $5.49 \times 10^{-4}$  kg/s, the zigzag channel has a relatively high  $Nu$  and pressure drop characteristics; the convection heat transfer coefficient and Fanning friction coefficient for the zigzag channel with radian are the smallest. The pressure drop and the heat transfer performance decrease with the increase of the inserted straight channel length. The  $Nu$  and Fanning friction coefficient of the different channel shapes decrease with the increasing mass flow rate.
  - (5) The PEC of the zigzags with the inserted straight channels and the zigzag channel with radian are greater than 1, and the values are higher at lower mass flow rates, indicating that the best heat transfer performances are those in the zigzags with the inserted straight channels and the zigzag channel with radian. Additionally, the PEC are higher at lower mass flow rates. Moreover, the zigzag with the 4 mm inserted straight channel has a higher heat transfer performance.

**Author Contributions:** Conceptualization and supervision, Z.Z.; formal analysis and data curation, Y.Z.; validation, methodology, and software, X.M., X.C., S.L., S.Y., and Z.Z.; writing—original draft preparation, Y.Z. and Z.Z.

**Funding:** The authors gratefully acknowledge that this work was supported by the Jiangsu marine and fishery science and technology innovation and extension project (HY2017-8) and the Zhenjiang funds for the key research and development project (GY2016002-1).

**Conflicts of Interest:** The authors declare no conflict of interest.

## Nomenclature

$T$	Temperature (K)
$P$	Pressure (Pa)
$L$	length of channel (mm)
$f$	Fanning friction factor
$v$	Velocity (m/s)
$h$	Convective heat transfer coefficient ( $W/(m^2 \cdot K)$ )
$Nu$	Nusselt number
$C_p$	Specific heat ( $kJ/(kg \cdot K)$ )
$D_h$	hydraulic diameter (m)
$G$	mass flow rate (kg/s)
$\Delta P$	pressure drop (Pa)
$\Delta P_f$	pressure drop due to friction (Pa)
$\Delta P_a$	pressure drop due to acceleration (Pa)
PEC	Performance Evaluation Criteria

## Greek symbols

$\mu$	viscosity ( $Pa \cdot s$ )
$\rho$	density ( $kg/m^3$ )
$\lambda$	thermal conductivity ( $W/m \cdot K$ )

## Subscript

$w$	Wall
$b$	Bulk mean
$in$	inlet
$out$	outlet

## References

1. Zhang, P.; Ma, T.; Ke, H.; Wang, W.; Lin, Y.; Wang, Q. Numerical investigation on local thermal characteristics of printed heat exchanger for natural gas liquefaction. *Energy Procedia* **2019**, *158*, 5408–5413. [[CrossRef](#)]
2. Morteau, M.V.V.; Paiva, K.V.; Mantelli, M.B.H. Diffusion bonded cross-flow compact heat exchangers: Theoretical predictions and experiments. *Int. J. Therm. Sci.* **2016**, *110*, 285–298. [[CrossRef](#)]
3. Yoon, S.H.; No, H.C.; Kang, G.B. Assessment of straight, zigzag, S-shape, and airfoil PCHEs for intermediate heat exchangers of HTGRs and SFRs. *Nucl. Eng. Des.* **2014**, *270*, 334–343. [[CrossRef](#)]
4. Zhao, Z.; Zhang, X.; Zhao, K.; Jiang, P.; Chen, Y. Numerical investigation on heat transfer and flow characteristics of supercritical nitrogen in a straight channel of printed circuit heat exchanger. *Appl. Therm. Eng.* **2017**, *126*, 717–729. [[CrossRef](#)]
5. Huang, C.; Cai, W.; Wang, Y.; Liu, Y.; Li, Q.; Li, B. Review on the characteristics of flow and heat transfer in printed circuit heat exchangers. *Appl. Therm. Eng.* **2019**, *153*, 190–205. [[CrossRef](#)]
6. Chen, M.; Sun, X.; Christensen, R.N.; Shi, S.; Skavdahl, I.; Utgikar, V.; Sabharwall, P. Experimental and numerical study of a printed circuit heat exchanger. *Ann. Nucl. Energy* **2016**, *97*, 221–231. [[CrossRef](#)]
7. Mylavarapu, S.K.; Sun, X.; Glosup, R.E.; Christensen, R.N.; Patterson, M.W. Thermal hydraulic performance testing of printed circuit heat exchangers in a high-temperature helium test facility. *Appl. Therm. Eng.* **2014**, *65*, 605–614. [[CrossRef](#)]
8. Chen, M.; Sun, X.; Christensen, R.N.; Skavdahl, I.; Utgikar, V.; Sabharwall, P. Dynamic behavior of a high-temperature printed circuit heat exchanger: Numerical modeling and experimental investigation. *Appl. Therm. Eng.* **2018**, *135*, 246–256. [[CrossRef](#)]
9. Zheng, Z.; Fletcher, D.F.; Haynes, B.S. Transient laminar heat transfer simulations in periodic zigzag channels. *Int. J. Heat Mass Transf.* **2014**, *71*, 758–768. [[CrossRef](#)]
10. Lee, S.M.; Kim, K.Y. Optimization of zigzag flow channels of a printed circuit heat exchanger for nuclear power plant application. *J. Nucl. Sci. Technol.* **2012**, *49*, 343–351. [[CrossRef](#)]
11. Kim, I.H.; No, H.C. Physical model development and optimal design of PCHE for intermediate heat exchangers in HTGRs. *Nucl. Eng. Des.* **2012**, *243*, 243–250. [[CrossRef](#)]
12. Yang, Y.; Li, H.; Yao, M.; Gao, W.; Zhang, Y.; Zhang, L. Investigation on the effects of narrowed channel cross-sections on the heat transfer performance of a wavy-channeled PCHE. *Int. J. Heat Mass Transf.* **2019**, *135*, 33–43. [[CrossRef](#)]
13. Tsuzuki, N.; Kato, Y.; Nikitin, K.; Ishizuka, T. Advanced Microchannel Heat Exchanger with S-shaped Fins. *J. Nucl. Sci. Technol.* **2009**, *46*, 403–412. [[CrossRef](#)]
14. Chu, W.X.; Li, X.H.; Ma, T.; Chen, Y.T.; Wang, Q.W. Study on hydraulic and thermal performance of printed circuit heat transfer surface with distributed airfoil fins. *Appl. Therm. Eng.* **2017**, *114*, 1309–1318. [[CrossRef](#)]
15. Zhang, H.; Guo, J.; Huai, X.; Cheng, K.; Cui, X. Studies on the thermal-hydraulic performance of zigzag channel with supercritical pressure CO<sub>2</sub>. *J. Supercrit. Fluids* **2019**, *148*, 104–115. [[CrossRef](#)]
16. Zhao, Z.; Zhao, K.; Jia, D.; Jiang, P.; Shen, R. Numerical Investigation on the Flow and Heat Transfer Characteristics of Supercritical Liquefied Natural Gas in an Airfoil Fin Printed Circuit Heat Exchanger. *Energies* **2017**, *10*, 1828. [[CrossRef](#)]
17. Huang, D.; Wu, Z.; Sunden, B.; Li, W. A brief review on convection heat transfer of fluids at supercritical pressures in tubes and the recent progress. *Appl. Energy* **2016**, *162*, 494–505. [[CrossRef](#)]
18. Kim, D.E.; Kim, M.H.; Cha, J.E.; Kim, S.O. Numerical investigation on thermal-hydraulic performance of new printed circuit heat exchanger model. *Nucl. Eng. Des.* **2008**, *238*, 3269–3276. [[CrossRef](#)]
19. Sung, J.; Lee, J.Y. Effect of tangled channels on the heat transfer in a printed circuit heat exchanger. *Int. J. Heat Mass Transf.* **2017**, *115*, 647–656. [[CrossRef](#)]
20. Baek, S.; Kim, J.H.; Jeong, S.; Jung, J. Development of highly effective cryogenic printed circuit heat exchanger (PCHE) with low axial conduction. *Cryogenics* **2012**, *52*, 366–374. [[CrossRef](#)]
21. Lee, S.M.; Kim, K.Y.; Kim, S.W. Multi-objective optimization of a double-faced type printed circuit heat exchanger. *Appl. Therm. Eng.* **2013**, *60*, 44–50. [[CrossRef](#)]
22. Jeon, S.; Baik, Y.J.; Byon, C.; Kim, W. Thermal performance of heterogeneous PCHE for supercritical CO<sub>2</sub> energy cycle. *Int. J. Heat Mass Transf.* **2016**, *102*, 867–876. [[CrossRef](#)]
23. Zhao, Z.; Zhou, Y.; Ma, X.; Chen, X.; Li, S.; Yang, S. Numerical Study on Thermal Hydraulic Performance of Supercritical LNG in Zigzag-Type Channel PCHEs. *Energies* **2019**, *12*, 548. [[CrossRef](#)]

24. Rogala, Z.; Brenk, A.; Malecha, Z. Theoretical and Numerical Analysis of Freezing Risk during LNG Evaporation Process. *Energies* **2019**, *12*, 1426. [[CrossRef](#)]
25. Higashi, Y. NIST Thermodynamic and Transport Properties of Refrigerants and Refrigerant Mixtures (REFPROP). *Netsu Bussei* **2000**, *4*, 1575.
26. Safaei, M.R.; Togun, H.; Vafai, K.; Kazi, S.N.; Badarudin, A. Investigation of Heat Transfer Enhancement in a Forward-Facing Contracting Channel Using FMWCNT Nanofluids. *Numer. Heat Transf. Appl.* **2014**, *66*, 1321–1340. [[CrossRef](#)]



© 2019 by the authors. Licensee MDPI, Basel, Switzerland. This article is an open access article distributed under the terms and conditions of the Creative Commons Attribution (CC BY) license (<http://creativecommons.org/licenses/by/4.0/>).